Bulgarian Chemical Communications, Volume 50, Special Issue F (pp. 205–210) 2018

Characterization of in-situ-sampled particulate matter in air pollution localized by lidar monitoring

I. V. Grigorov[1], G. V. Kolarov[1], L. L. Gurdev[1], Z. P. Cherkezova-Zheleva[2], L. S. Slavov[1], Ch. G. Ghelev[1], R. V. Ilieva[3], M. V. Iliev[3], V. I. Groudeva[3], D. V. Stoyanov[1], I. I. Nedkov[1*]

[1] *Institute of Electronics, Bulgarian Academy of Sciences, 72, Tsarigradsko Chaussee blvd., 1784 Sofia, Bulgaria*
[2] *Institute of Catalysis, Bulgarian Academy of Sciences, Acad. G. Bonchev str., bl. 11, 1113 Sofia, Bulgaria*
[3] *Faculty of Biology, St. Kl. Ohridski University of Sofia, 8, Dragan Tsankov blvd., 1164 Sofia, Bulgaria*

Received October 30, 2018; Accepted December 10, 2018

The work presents part of comprehensive studies performed during 2018 that dealt with particulate matter (PM), more specifically such with size ≤ 10 μm (PM10) and ≤ 2.5 μm (PM2.5), in the atmospheric aerosol. The experiments combined lidar monitoring over a densely populated urban area (city of Sofia, capital of Bulgaria) with on-the-spot sampling at sites with high concentration of dust products. Once the place of high PM concentration was localized by the lidar, samples were taken using a Hygitest 106 (Maimex) – a high-efficiency portable device for sampling and concentration determination of PM in atmospheric aerosol. X-ray diffraction and Mössbauer studies at room temperature were used to study the PM inorganic part. The material collected was also subjected to microbiological investigation by first applying a standard procedure for isolation of pure microbial cultures. The bacterial and fungal obtained isolates were identified on the basis of their morphological, physiological and biochemical characteristics. Thus, it was found that the surface of the micron-sized particles can adsorb both mechanical and microbial contaminants, while the liquid envelope, when the PM is dispersed as aerosols, may preserve this nano-world and, in some cases, create conditions favoring the occurrence of chemical and bio-processes. The lidar maps constructed can be further used for tracing the full air mass transport carrying contamination from a number of pollution sources (chemical, biological, dust, etc.), distributed over the scanned region.

Keywords: lidar monitoring, particulate matter, bio-aerosols, air quality.

INTRODUCTION

Particulate matter (PM) air pollution originates from different sources and has different chemical and physical properties [1, 2]. Monitoring ambient levels of PM facilitates the planning of effective control strategies to combat urban pollution. Lidar mapping data can add synoptic information and visualization to ground-based air-quality data modeling. Together, the integrated data increase the usefulness of any single dataset. However, the recent research and policy emphasis on regional and intercontinental transport of air pollutants, such as fine particulate matter smaller than 10 μm and 2.5 μm in diameter (PM_{10} and $PM_{2.5}$), has highlighted the need for additional data sources to monitor air pollution as it moves in multiple dimensions, both spatially and temporally. The combination of lidar remote sensing and ground-based PM monitoring data can form the basis of an integrated air-quality characterization [3].

The research described here pertains to the air pollution of the city of Sofia (capital of Bulgaria), which was recently (2015) ranked as the 33rd most polluted city in a study including 157 European cities [4]. It is a continuation of our work on PM in the atmospheric aerosol over the city of Sofia and couples lidar monitoring over critical in terms of pollution urban areas, as determined by lidar sensing, with contact on-the-spot sampling. The city is located in a large valley surrounded by mountains hindering the processes of self-cleaning of the atmosphere. Moreover, a typical characteristic of the weather in the region are cold spells and calm atmosphere during the winter-spring transition period (months of February – May) resulting in temperature inversions that contribute to the already significant overall pollution over the city. Thus, we

* To whom all correspondence should be sent:
E-mail: nedkovivan@yahoo.co.uk

chose to study the air pollution on windless days at three city sites typical in terms of heavy traffic and altitude above sea level (ASL), two of them being adjacent to the Tsarigradsko Chaussee blvd. (the city's busiest thoroughfare) at four kilometers away from the city center, ASL 620 m [5] and within the central city area. The third site is adjacent to Dragan Tsankov blvd. (the building of the Faculty of Biology, University of Sofia, ASL 610 m) – another busy thoroughfare near the city center with heavy traffic during rush hours (average intensity according to Sofia Municipality of about 1000 vehicles per hour), interestingly forming a border between a densely populated residential district and a large park (Borisova Gradina).

METHODS, INSTRUMENTS AND PROCEDURES

The lidar mapping was performed by a lidar system installed on the roof of Institute of Electronics (eight kilometers from the city center); the site at Dragan Tsankov blvd. is located at a distance of 5.5 km from the lidar. This lidar system, developed in the Laser Radar Laboratory of the Institute of Electronics, is capable of scanning the horizontal and vertical aerosol distributions and transport of air masses with a spatial resolution of 30 m and a beam divergence of ~1omrad at operational distances of about 25 km. The laser emitter (wavelength of 510.6 nm) is a pulsed CuBr vapor laser, designed and built in the Institute of Solid-State Physics, Bulgarian Academy of Sciences, with a repetition rate of 10 KHz at a 15-ns pulse duration. The receiving system comprises a Carl Zeiss Jena Cassegrain telescope (aperture of 20 cm, a focal distance of 1 m), a 2-mm-wide focal diaphragm, an interference filter with 2-nm-wide passband, and an EMI 9789 photo-multiplier tube operating in a photon-counting mode. The receiving system is fully computerized for collecting and processing the lidar data using a PCO 1001 1024-channel digital interface system for signal strobing and accumulation. The strobe interval along the line of sight (LOS) is 30-m long.

The samples were taken using a Hygitest 106 (Maimex), a high-efficiency portable device for sampling and concentration determination of PM in atmospheric aerosol. The flow-rate of the aspirated air was measured by an analog unit, while the value of the sampled volume (300 m^3) through the filter was digitized by means of a six-bit ADC. The dust was collected on a filter (boro-silicon oxide) with #3 μm and #8 μm (FILTER-LAB, Material MCE, Lot.180509006 and 07). Additionally, the material collected on the filters after three hours of aspiration during the lidar monitoring was studied by SEM and EDAX. Mössbauer analysis was made using a Wissenschaftliche Elektronik GmbH apparatus, working at a constant acceleration mode; 57Co/Cr source, α-Fe standard. The parameters of hyperfine interactions of the Moessbauer spectral components were determined by computer fitting: isomer shift (IS), quadrupole splitting (QS), hyperfine effective magnetic field in the site of iron nuclei (H_{eff}), as well as line widths (FW) and component relative weights (G). In the experiments presented, we directed the lidar beam to the sites of contact sampling to probe the near-surface atmosphere in a horizontal direction. The measurement time covered practically the entire period of the evening traffic maximums, while maximums of the PM pollutions were clearly observed in the backscattered lidar signals, as received and processed by our system.

RESULTS AND DISCUSSION

Using the data for the mass concentration, M_a, acquired by the sampling device, we calibrated the two major lidar signal parameters, namely, the extinction coefficient $\alpha(r)$ and the backscattering coefficient $\beta(r)$ [6]. For the lidar ratio $LiR = \alpha(r)/\beta(r)$ we assumed the typical value $LiR = 50$ [7]. Under the condition of a homogeneous atmosphere in a horizontal plane, the parameters $\beta(r)$ and $\alpha(r)$ were calculated using the lidar equation:

$$P(r) = P_0 \frac{c\tau}{2} C \frac{\beta(r)}{r^2} \exp\left[-2\int_{r_0}^{r} \alpha(r')dr'\right], \quad (1)$$

where $P(r)$ is the power of detected laser radiation backscattered by the atmosphere from a distance $r = ct/t$, t being the time interval following the emission of the laser pulse, τ is the pulse duration, and C is a coefficient related to the specific physical and mechanical parameters of our equipment. Under the same assumption of homogeneity, the extinction coefficient $\alpha(r)$ is calculated by

$$\alpha(r) = -\frac{1}{2}\frac{dS(r)}{dr}, \quad (2)$$

where $S(r) = \ln [r^2 P(r)]$.

Figure 1 presents the dependence of the mass concentration M in mg/m^3 as a function of $\alpha(r)$ calculated using the data of all sampling measurements. The linear fit ($Y = A + BX$) shows a small, acceptable, value for the standard deviation (~0.01004, i.e., a relative error of less than 4%), while the correlation coefficient exceeds 0.99.

Figure 2 presents a series of successive in time horizontal lidar profiles arranged vertically and superimposed on the Google Sofia City map. As evi-

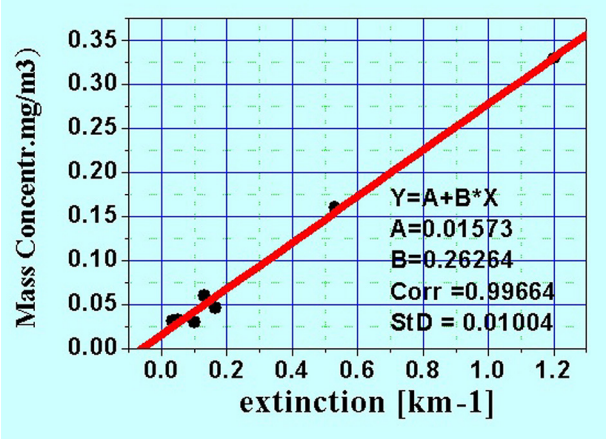

Fig. 1. LIDAR calibration curve in mass concentration as a function of the light extinction coefficient.

dent, one can determine the aerosol field distribution at each distance from the lidar station as well as at each moment (time resolution of 5 min) during the entire measuring time. Thus, these results demonstrate the possibility of a detailed fast remote monitoring of the air pollution over large urban regions, providing fast estimates of its transport over the city and determination of the pollution sources locations.

Figure 3 (a) and (b) below are SEM images of the material collected on the filters after three hours of aspiration during the lidar monitoring; they present a large amount of particles larger than 2.5 μm and a very limited amount of small particles (under 2.5 μm). Fig. 3(a) shows a typical shape of dust particles with sizes between 2.5 μm and 10 μm, which are of hybrid origin. Fig. 3(b) illustrates a wide variety of quasi spherical particles with an average size ≥2.5 μm. Fig. 3(c) shows a large (≥10 μm) particle. Fig. 3(d) is a histogram of the particles size distribution in the PM over Dragan Tsankov blvd., Sofia. The airborne PM can be divided into two classes, fine PM (particles 2.5 μm in diameter or smaller) and coarse PM (particles 2.5 μm to 10 μm in diameter), which differ not only in size, but also in source, chemical composition, physical properties, and formation process [2]. Major sources of $PM_{2.5}$ are fossil fuel combustion by industry, motor vehicles, residential fireplaces and wood stoves; vegetation burning; and smelting or other processing [8]. Examples of natural bio-aerosols suspended as $PM_{2.5}$ include bacteria, viruses, and endotoxins. Fungal spores, pollen, and plant and insect fragments are examples of natural bio-aerosols suspended as coarse PM [9]. The distribution of the PMs diameter varies from tens of nanometers to a more than 10 micrometers for pollen or plant debris [10–12]. After selecting typical particle images based on ten points on the filter's surface, the percentage distribution of the particles with different size was obtained: over 10 μm, from 2.5 μm up to 10 μm and less than 2.5 μm. (Fig. 3d).

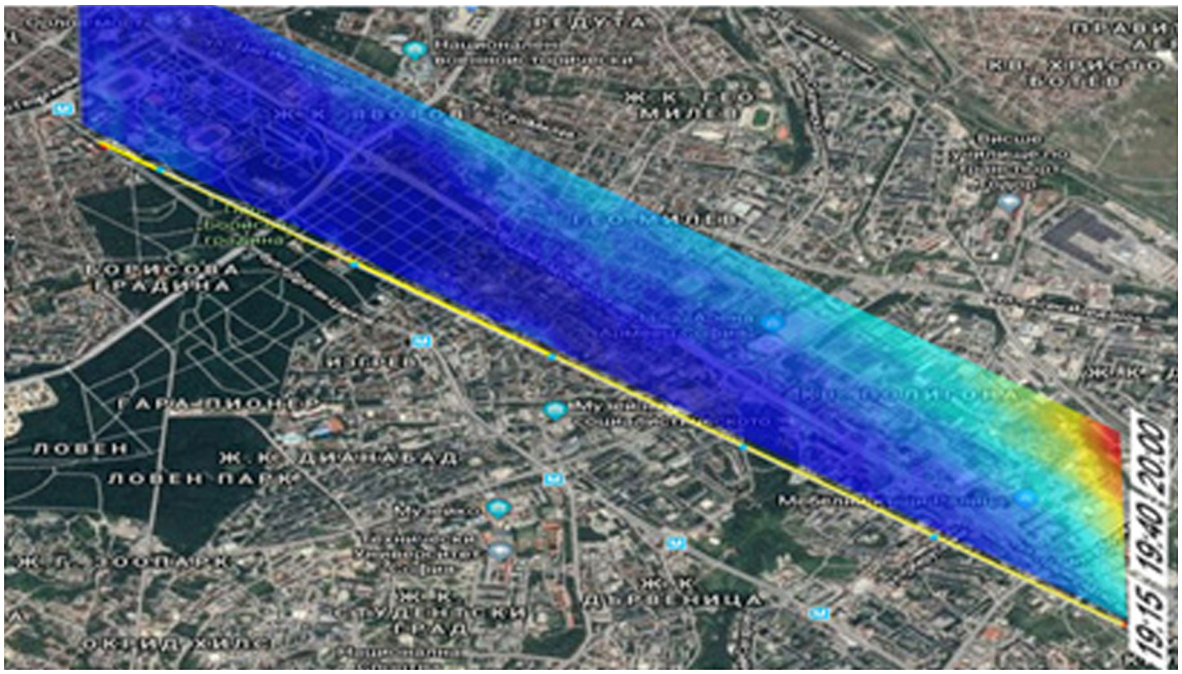

Fig. 2. Temporal evolution of attenuated backscattering profiles arranged in vertical. The warmer colors correspond to higher aerosol concentration.

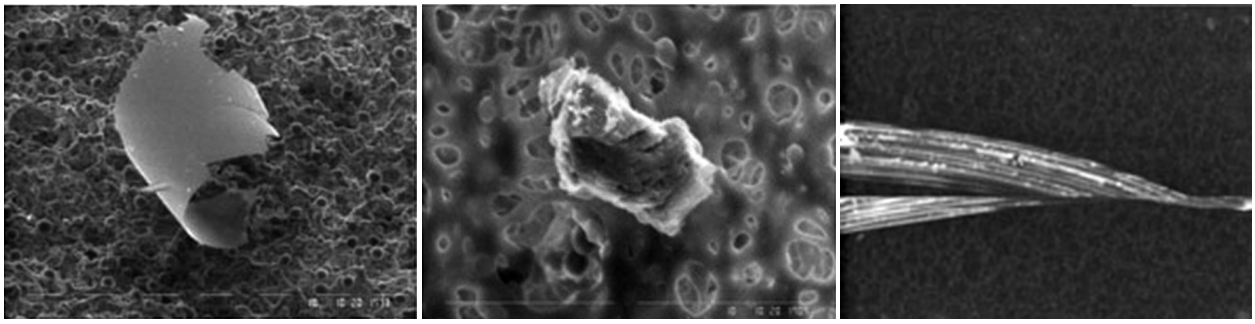

a) *b*) *c*)

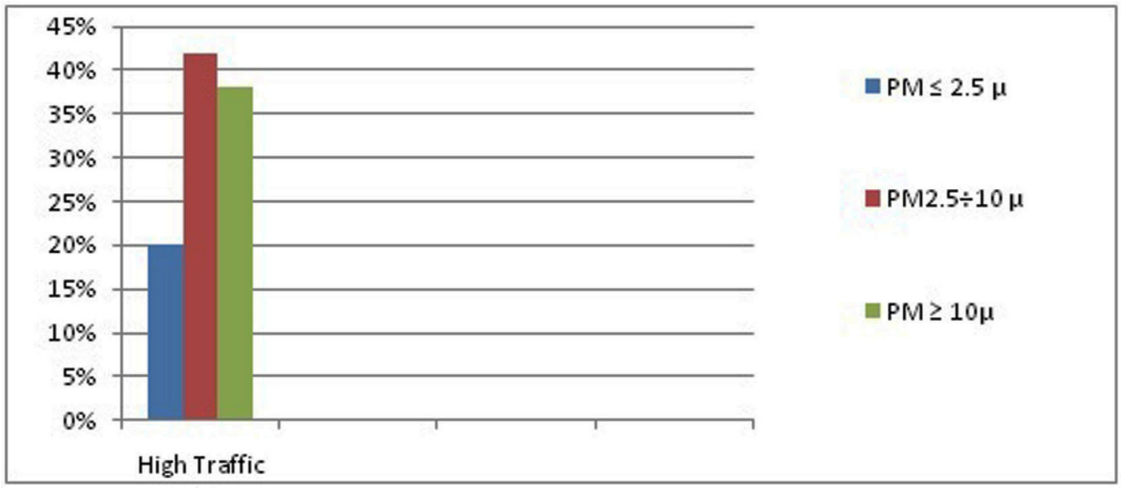

d)

Fig. 3. PM with sizes between 2.5 µm – 10 µm (*a*); PM with size ≥2.5 µm, the fibers reveal the filter structure (*b*); a large (≥10 µm) particle (*c*); and particles size distribution in PM over Dragan Tsankov blvd., Sofia (*d*).

The dry fraction of the material absorbed on the filters was studied by EDAX analysis for the presence of metals. The data (Fig. 4) showed the presence of Fe, Si, Pb, etc. Our attention was focused on iron, whose concentration was about 0.17 mg/m^3 per day, with the permissible limit being 0.04 mg/m^3.

The data obtained using Mössbauer spectroscopy revealed the presence of iron containing phases. The material collected near Dragan Tsankov blvd. has a complicated spectrum (see Fig. 5) in which magnetic and paramagnetic phases can be resolved, i.e. the spectrum is a superposition of sextet- and doublet-type components. The hyperfine parameters calculated after spectrum evaluation are presented in Table 1. The four sextet components observed in the spectrum have the hyperfine parameters values characteristic of iron oxide phases – hematite (Sxt1 = α-Fe_2O_3), magnetite (Sxt2 and Sxt3 = Fe_3O_4), as well as a metal iron phase of α-Fe (Sxt 4). The value obtained of the hyperfine effective magnetic field of this metal iron phase is lower than the one characteristic for bulk material, namely, 33 T [13]. It is well known that the relation between the hyperfine field and the magnetic particles volume can be expressed using the collective magnetic excitation (CME) model; in our case it reveals the pres-

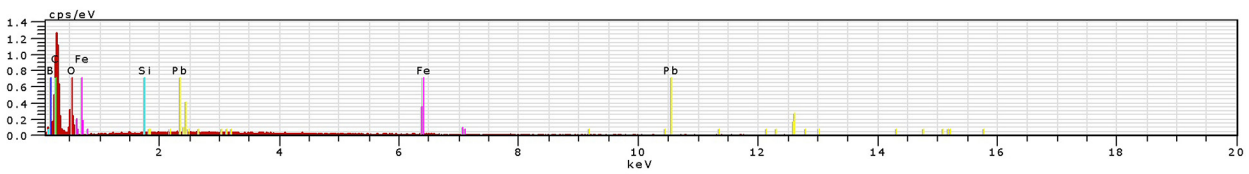

Fig. 4. EDAX data for powders from the investigated area.

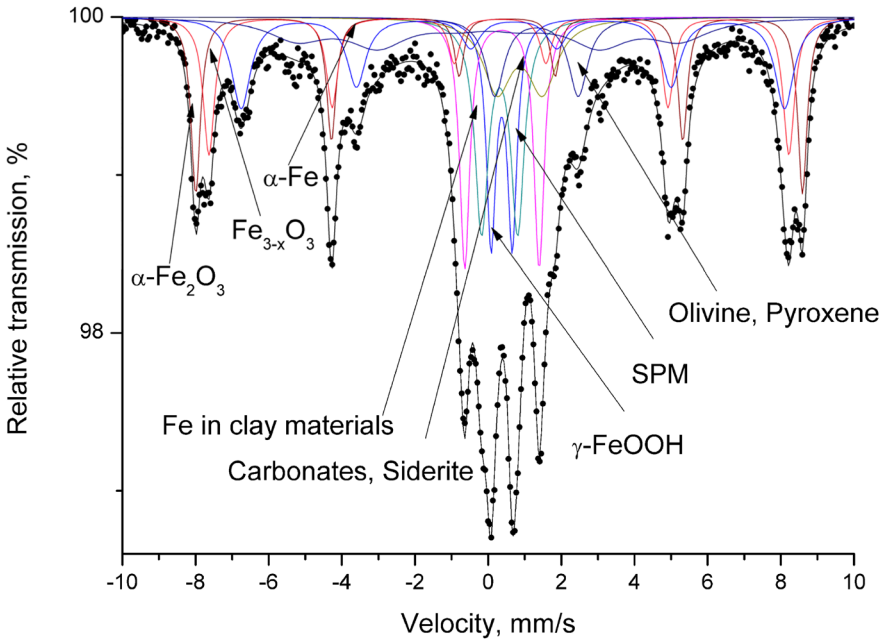

Fig. 5. Mössbauer spectra of sample collected at Dragan Tsankov blvd.

Table 1. Mössbauer parameters of sample collected at Dragan Tzankov blvd.

Components	IS, mm/s	QS, mm/s	Heff, T	FWHM, mm/s	G, %
Sxt1-α-Fe_2O_3	0.37	–0.11	51.5	0.32	14
Sxt2-$Fe_{3-x}O_4$	0.30	0.02	49.3	0.38	13
Sxt3-$Fe_{3-x}O_4$	0.68	0.01	46.2	0.62	15
Sxt4-α-Fe	0.00	0.00	32.5	1.70	13
Dbl1-γ-FeOOH	0.36	0.58	–	0.32	8
Dbl2-SPM	0.31	0.99	–	0.44	12
Dbl3-Fe in clay materials	0.37	2.04	–	0.33	11
Dbl4-Carbonates, Siderite	0.88	1.24	–	0.82	8
Dbl5-Olivine, Pyroxene	1.31	2.28	–	0.62	6

ence of highly-dispersed particles (grain size below 30 nm) [14]. On the other hand, the doublet components could be connected mainly with the presence of Fe in clay materials (Dbl3) and iron oxide or oxi-hydroxide phases with a grain size lower than 20 nm, which exhibit a superparamagnetic behavior (Dbl2). The hyperfine parameters calculated of the other doublet components reveal the presence of Fe^{3+} in a lepidicrocite phase (Dbl1=FeOOH), Fe^{2+} in carbonate or siderite phases (Db4) and Fe^{2+} in olivine or pyroxene (Dbl5). This is due to the presence of materials formed at the earth's surface (sediments, soils, clays, etc.). In regard to the magnetic phases, we believe that the magnetite originates from automobile exhaust, while the metallic iron is produced by the friction between streetcars wheels and the rails of the streetcar route passing near the air sampling site.

The PM material collected was subjected also to microbiological analysis by applying a standard procedure for isolation of pure microbial cultures. The bacterial and fungal isolates obtained were identified on the basis of morphological, physiological and biochemical characteristics. A molecular approach, including the amplification of 16S rDNA, resp. 18S rDNA for fungal isolates, was also used. The microbiological survey of the atmosphere of the densely populated part of Sofia city indicated that the particulate matter collected harbors a variety of different viable microorganisms. The majority of the bacterial isolates was presented by predominantly saprophytic pigmented bacteria, mainly from

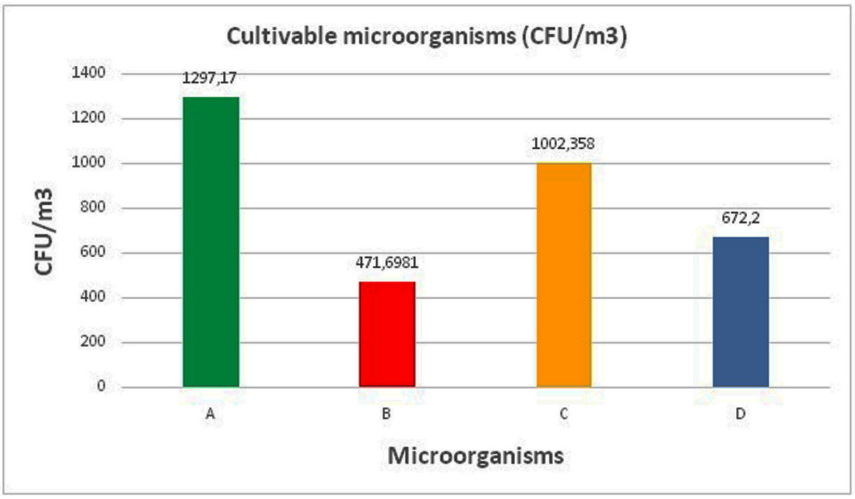

Fig. 6. Number of microorganisms (CFU/m^3) detected at the sampling point: from left to right – heterotrophic aerobic bacteria; oligotrophic microorganisms; fungi; spore-forming bacteria.

the genus *Micrococcus* (66%). The genus *Bacillus* was also abundant, presented by representatives of the species *B. pumilus*, *B. cereus*, *B. thuringensis* and *B. cereus*. One isolate was determined as *Staphylococcus equorum*. The fungal presence was expressed mainly by the genera *Penicillium* and *Aspergillus*. Two of the isolates were related to the genera *Cladosporium* and *Symmetrospora*. Figure 6 shows the origin of the organic contamination absorbed on the particles and the estimated number of viable microorganisms in colony-forming units (CFU).

CONCLUSIONS

Combining lidar monitoring with *in-situ* sampling represents an effective first step toward the creation of a highly informative near-real-time monitoring system for a complex analysis of the air quality. This investigation shows that the surface of the micron-sized particles can adsorb both mechanical and microbial contaminants, while the liquid envelope, when the PM is dispersed as aerosols, may preserve this nano-world and, in some cases, create conditions favoring the occurrence of chemical and bio-processes. The lidar maps constructed can be further used for tracing the full air-mass transport, carrying contamination from a number of pollution sources (chemical, biological, dust, etc.), distributed over the scanned region. Further, the sampling schedule should be so chosen as to reveal any characteristic seasonal hazardous contamination.

Acknowledgment: *This work was financed in part under contract DN 18/16 with the National Science Fund, Bulgaria, and included in the European Program of the COST Action CA16202.*

REFERENCES

1. S. Fuzzi, U. Baltensperger, K. Carslaw, S. Decesari, H. Denier Van Der Gon, M. C. Facchini, D. Fowler, I. Koren, B. Langford, U. Lohmann, E. Nemitz, E., *Atmos. Chem. Phys.*, **15** (14), 8217 (2015).
2. L. Raisi, M. Lazaridis, E. Katsivela, *Global NEST J.*, **12** (1), 84 (2010).
3. C. Mazzoleni, *Remote Sensing*, **2** (4), 1077 (2010).
4. http://www.nsi.bg/nrnm/show2.php?sid=57422&ezik=bul&e=128142
5. L. Slavov, M. Iliev, R. Ilieva, R. Angelova, Ch. Ghelev, I. Grigorov, G. Kolarov, L . Gurdev V. Grudeva, D. Stoyanov, I. Nedkov, *Machines Technol. Mater.*, **12** (10), 412 (2018).
6. Al. Carswell, *Can. J. Phys.*, **61**, 378 (1983).
7. D. Althausen, R. Engelmann, B. Holger, B. Heese, A. Ansmann, D. Mueller, *J. Atmos. Oceanic Technol.*, **26,** 2366 (2009).
8. World Health Organization, Health effects of particulate matter (ISBN 978 92 890 0001 7), 2013.
9. J. Fröhlich-Nowoisky, D. A. Pickersgill, V. R. Després, U. Pöschl, in: *Proc. Nat. Acad. Sci.*, **106** (31), 12814 (2009).
10. R. Jaenicke, *Science*, **308** (5718), 73 (2005).
11. William C. Hinds, Aerosol technology: properties, behavior, and measurement of airborne particles, John Wiley & Sons, 2012.
12. U. Pöschl, *Angew. Chem. Int. Ed.*, **44** (46), 7520 (2005).
13. B. Fultz, in: Characterization of Materials. E. Kaufmann, Wiley, New York, 2011.
14. U. Schwertmann, R. M. Cornell, C. B. Koch, Iron Oxides in the Laboratory: Preparation and Characterization, 3rd Edition, Wiley, New York, 2017.